

A COMPUTATIONALLY EFFICIENT MULTIDIMENSIONAL VISION TRANSFORMER

A. ELICHI*, K. JBILOU*, AND F. DUFRENOIS†

Abstract. Vision Transformers have achieved state-of-the-art performance in a wide range of computer vision tasks, but their practical deployment is limited by high computational and memory costs. In this paper, we introduce a novel tensor-based framework for Vision Transformers built upon the *Tensor Cosine Product* (c-product). By exploiting multilinear structures inherent in image data and the orthogonality of cosine transforms, the proposed approach enables efficient attention mechanisms and structured feature representations. We develop the theoretical foundations of the tensor cosine product, analyze its algebraic properties, and integrate it into a new c-product-based Vision Transformer architecture (TCP-ViT). Numerical experiments on standard classification and segmentation benchmarks demonstrate that the proposed method achieves a uniform $1/C$ parameter reduction (where C is the number of channels) while maintaining competitive accuracy.

1 Introduction Vision Transformers (ViTs) [3] have recently attracted considerable interest as a strong alternative to convolutional neural networks, owing to their ability to capture long-range dependencies via self-attention. Unlike convolutional architectures, which operate on local receptive fields with shared weights, ViTs facilitate global information exchange across the entire image from the earliest network layers. This global modeling capability has enabled ViTs to achieve state-of-the-art performance across a wide range of computer vision tasks, including image classification, object detection, and semantic segmentation.

Despite these successes, conventional ViT models suffer from several intrinsic limitations. Images are first divided into patches that are subsequently flattened into vectors and processed as independent tokens. This vectorization step disrupts the inherent multidimensional structure of image data and neglects correlations across spatial and channel dimensions. In addition, the self-attention mechanism exhibits quadratic computational and memory complexity with respect to the number of tokens, rendering ViTs costly to train and deploy on high-resolution images. These factors significantly constrain their scalability and practicality in resource-limited environments.

To alleviate these issues, extensive research has been devoted to the development of efficient Vision Transformer variants. Proposed approaches include sparse and axial attention mechanisms, low-rank and kernel-based attention formulations, as well as hybrid architectures that combine convolutional and transformer components [28, 29, 30]. Although these methods reduce computational overhead, they generally retain vectorized representations and do not explicitly exploit the multilinear structure of visual data. Consequently, important spatial and spectral relationships may remain underutilized.

Recent advances in tensor numerical linear algebra provide an alternative and mathematically principled approach to addressing these challenges. Tensors offer natural representations for multidimensional data and support algorithms that preserve structural properties while reducing redundancy [11, 14, 17]. In particular, tensor products based on orthogonal transforms, such as Fourier and cosine transforms, have demonstrated strong effectiveness in large-scale inverse problems, regularization of ill-posed systems, and high-dimensional scientific computing [1, 5]. These techniques benefit from solid theoretical foundations and efficient implementations enabled by fast transform algorithms.

Motivated by these developments, we propose an efficient Vision Transformer framework based on the *tensor cosine product* (c-product). By operating directly on tensor-valued representations and employing cosine-transform-based tensor products, the proposed method preserves spatial structure, reduces computational complexity, and avoids the use of complex-valued arithmetic. The cosine transform is particularly well suited for vision applications due to its strong energy compaction properties and favorable boundary behavior [21].

The tensor cosine product enables a structured formulation of attention mechanisms in which interactions between image patches are computed within a multilinear transform domain. This formulation leads to more efficient attention computation, improved memory utilization, and a natural integration of numerical linear algebra techniques into modern deep learning architectures [7].

The main contributions of this work are summarized as follows:

- We formally define the tensor cosine product and establish its fundamental algebraic and orthogonality-preserving properties.

*Université du Littoral Cote d’Opale, LMPA, 50 rue F. Buisson, 62228 Calais-Cedex, France.

† LISIC, 50 rue F. Buisson, Université du Littoral Cote d’Opale, 62228 Calais-Cedex, France.

- We introduce a c-product-based self-attention mechanism that preserves tensor structure while reducing computational and memory complexity.
- We design a cosine-product Vision Transformer (TCP-ViT) that operates directly on tensor-valued image patches, achieving a uniform $1/C$ parameter reduction across all linear components.
- We provide theoretical complexity analysis and numerical experiments demonstrating the efficiency and competitiveness of the proposed approach.

The remainder of this paper is structured as follows. Section 2 reviews related work on efficient Vision Transformers and tensor methods in deep learning. Section 3 introduces the discrete cosine transform and the tensor cosine product with its algebraic properties. Section 4 recalls the standard Vision Transformer architecture and establishes the notation used throughout. Section 5 presents the tensorized TCP-ViT architecture. Section 6 provides the parameter efficiency and computational complexity analyses. Section 7 reports numerical experiments. Section 8 concludes the paper.

2 Related Work

2.1 Efficient Vision Transformers. The original ViT [3, 13] demonstrated that pure transformer architectures can match or exceed CNNs on image classification when trained on large-scale datasets. However, its quadratic attention cost motivated numerous efficient variants. DeiT [28] introduced knowledge distillation and data-efficient training strategies. Swin Transformer [19] employs shifted window attention to achieve linear complexity in the number of tokens. Axial attention [29] factorizes the full attention along spatial axes. These approaches reduce computational cost but retain the vectorized token representation and do not explicitly leverage the multilinear structure of image data.

2.2 Tensor Methods in Deep Learning. Tensor decompositions have been widely applied to compress neural networks. Tucker decomposition [16] and tensor-train (TT) [23] formats have been used to factorize weight matrices in fully connected and convolutional layers, achieving significant parameter reductions. LASER [25] showed that applying SVD to individual weight matrices and removing components corresponding to the smallest singular values can improve LLM reasoning, particularly when compressing the feed-forward network. More recently, the t-product framework [14, 15] has enabled structured tensor operations based on the discrete Fourier transform (DFT), with applications to tensor regression, principal component analysis [10, 4], and inverse problems [6, 5]. The present work adopts the cosine-transform variant of the t-product, which operates entirely in the real domain and avoids the complex arithmetic inherent to DFT-based methods.

2.3 Tensor-based Attention Compression. The most closely related work is TensorLLM [9], which tensorises multi-head attention weights by stacking the per-head query, key, value, and output matrices into a 4D tensor and applying Tucker decomposition with shared factor matrices across heads. While both our approach and TensorLLM exploit the multi-head structure of attention, the two methods differ fundamentally in three respects. First, TensorLLM is a *post-hoc* compression technique: it decomposes pre-trained weights via an approximate low-rank factorization, which introduces approximation error controlled by the chosen multilinear ranks. In contrast, our c-product formulation is a *native algebraic reformulation*: the model is trained directly with the c-product, and the resulting factorization is *exact*, with parameter reduction arising from the block-diagonal structure rather than from rank truncation. Second, TensorLLM requires hyperparameter selection for the multilinear ranks and produces variable compression ratios depending on the chosen ranks, whereas the c-product yields a *uniform, architecture-independent* parameter reduction that is determined solely by the number of channels. Third, the cross-channel coupling mechanism differs: TensorLLM learns shared factor matrices at additional computational cost, while the c-product couples channels *implicitly* through the fixed orthogonal DCT matrix Φ_C at zero parametric cost.

In a related but distinct direction, Su et al. [26] proposed DctViT, a hybrid CNN–Transformer architecture that employs the DCT for feature map compression within a dedicated convolutional block (DAD block). Their approach applies the DCT as a signal processing tool to reduce spatial redundancy in intermediate representations, while retaining a standard Transformer encoder with conventional matrix multiplications. In contrast, the present work uses the DCT as the algebraic foundation of a tensor product (\star_c) that replaces *all* linear projections in the Transformer encoder, yielding a principled and uniform $1/C$ parameter reduction across the entire architecture without any convolutional component.

3 The Cosine Product and Its Properties We begin by introducing the notation and definitions that will be used throughout the paper.

3.1 Notation Scalars are denoted by lowercase letters (a), vectors by bold lowercase letters (\mathbf{x}), matrices by uppercase letters (X), and third-order tensors by calligraphic letters (\mathcal{X}). The notation and symbols used throughout this paper are summarized in Table 3.1.

TABLE 3.1
Summary of notation used throughout the paper.

Symbol	Description
$H_{\text{img}}, W_{\text{img}}$	Image height and width
C	Number of image channels (tube dimension)
P	Patch side length
$N = H_{\text{img}}W_{\text{img}}/P^2$	Number of patches (tokens)
$d = P^2$	Spatial embedding dimension per frontal slice
$d_{\text{eff}} = d \cdot C$	Effective (flattened) embedding dimension
H	Number of attention heads
$d_h = d/H$	Per-head dimension (TCP-ViT); $d_h^{\text{std}} = d_{\text{eff}}/H$ (Std-ViT)
r_{ff}	FFN expansion ratio ($d_{\text{ff}} = r_{\text{ff}} \cdot d$)
L	Number of Transformer layers
\star_c	Tensor cosine product
$\mathcal{X}^{(k)}$	k -th frontal slice of \mathcal{X}
$\widehat{\mathcal{X}}^{(k)}$	k -th frontal slice of $\text{DCT}_3(\mathcal{X})$
\mathcal{X}^{\top_c}	Tensor c-transpose (Definition 3.2)

A third-order tensor is denoted by $\mathcal{X} \in \mathbb{R}^{m \times n \times C}$, where C denotes the size along the third mode (the tube dimension). The k -th frontal slice is written $\mathcal{X}^{(k)} \in \mathbb{R}^{m \times n}$ for $k = 1, \dots, C$.

3.2 Discrete Cosine Transform The orthogonal DCT-II matrix $\Phi_C \in \mathbb{R}^{C \times C}$ has entries defined by [8]

$$(\Phi_C)_{j,k} = \begin{cases} \sqrt{\frac{1}{C}}, & j = 0, \\ \sqrt{\frac{2}{C}} \cos\left[\frac{\pi(2k+1)j}{2C}\right], & j = 1, 2, \dots, C-1, \end{cases} \quad (3.1)$$

for $j, k = 0, 1, \dots, C-1$. It satisfies the orthogonality property

$$\Phi_C^\top \Phi_C = I_C, \quad \Phi_C \Phi_C^\top = I_C. \quad (3.2)$$

For a third-order tensor $\mathcal{X} \in \mathbb{R}^{m \times n \times C}$, the DCT along the third mode is defined as

$$\widehat{\mathcal{X}} = \text{DCT}_3(\mathcal{X}) = \mathcal{X} \times_3 \Phi_C, \quad (3.3)$$

where \times_3 denotes the mode-3 product. The k -th frontal slice of the transformed tensor is denoted $\widehat{\mathcal{X}}^{(k)}$ for $k = 1, \dots, C$. The inverse transform is

$$\mathcal{X} = \text{IDCT}_3(\widehat{\mathcal{X}}) = \widehat{\mathcal{X}} \times_3 \Phi_C^\top. \quad (3.4)$$

The DCT possesses several properties that make it particularly suitable for tensor-based vision transformers:

- *Energy compaction*: Most of the signal energy is concentrated in the low-frequency coefficients, enabling effective low-rank approximation and compression.
- *Real-valued orthogonality*: Unlike the Fourier transform, the DCT produces real-valued orthogonal coefficients, simplifying computations in neural networks.
- *Fast computation*: Using the fast cosine transform, the DCT can be computed in $O(C \log C)$ operations per tube, and $O(mnC \log C)$ for a third-order tensor along the third mode.
- *Invertibility*: The DCT is perfectly invertible, ensuring no information loss when transforming between the spatial and cosine domains.

3.3 Tensor Cosine Product DEFINITION 3.1 (Tensor Cosine Product). Let $\mathcal{A} \in \mathbb{R}^{m \times n \times C}$ and $\mathcal{B} \in \mathbb{R}^{n \times \ell \times C}$. The tensor cosine product (*c-product*) is defined as

$$\mathcal{C} = \mathcal{A} \star_c \mathcal{B} = \text{IDCT}_3\left(\text{DCT}_3(\mathcal{A}) \cdot \text{DCT}_3(\mathcal{B})\right) \in \mathbb{R}^{m \times \ell \times C}, \quad (3.5)$$

where the matrix product “ \cdot ” is performed slice-wise in the transform domain: $\widehat{\mathcal{C}}^{(k)} = \widehat{\mathcal{A}}^{(k)} \widehat{\mathcal{B}}^{(k)}$ for $k = 1, \dots, C$.

This product allows efficient computation via fast DCT algorithms, orthogonality-preserving operations for numerical stability, and structured low-rank approximations.

3.4 Basic Tensor Operations We summarize the fundamental definitions of third-order tensor operations under the c-product framework, extending the t-product algebra introduced by Kilmer et al. [14].

DEFINITION 3.2 (Tensor c-transpose). Let $\mathcal{A} \in \mathbb{R}^{m \times n \times C}$. The c-transpose $\mathcal{A}^{\top_c} \in \mathbb{R}^{n \times m \times C}$ is the tensor whose frontal slices in the DCT domain satisfy

$$\left(\widehat{\mathcal{A}^{\top_c}}\right)^{(k)} = \left(\widehat{\mathcal{A}}^{(k)}\right)^{\top}, \quad k = 1, \dots, C. \quad (3.6)$$

Equivalently, $\mathcal{A}^{\top_c} = \text{IDCT}_3\left(\text{DCT}_3(\mathcal{A})^{\top_{\text{slice}}}\right)$, where \top_{slice} transposes each frontal slice independently.

DEFINITION 3.3 (Identity tensor, orthogonality, invertibility). Let $\mathcal{A} \in \mathbb{R}^{m \times m \times C}$. Then:

(i) The identity tensor $\mathcal{I}_{m,C} \in \mathbb{R}^{m \times m \times C}$ is defined by requiring that its first frontal slice equals the $m \times m$ identity matrix I_m and all remaining frontal slices are zero.

Property: All frontal slices of $\widehat{\mathcal{I}}_{m,C} = \text{DCT}_3(\mathcal{I}_{m,C})$ coincide with I_m .

(ii) A tensor $\mathcal{Q} \in \mathbb{R}^{m \times m \times C}$ is c-orthogonal if $\mathcal{Q}^{\top_c} \star_c \mathcal{Q} = \mathcal{Q} \star_c \mathcal{Q}^{\top_c} = \mathcal{I}_{m,C}$.

(iii) A tensor \mathcal{Q} is f-orthogonal if each frontal slice $\widehat{\mathcal{Q}}^{(k)}$ of its DCT transform is an orthogonal matrix.

(iv) A tensor $\mathcal{Q} \in \mathbb{R}^{m \times m \times C}$ is f-diagonal if all frontal slices of $\widehat{\mathcal{Q}}$ are diagonal matrices.

(v) A tensor $\mathcal{A} \in \mathbb{R}^{m \times m \times C}$ is invertible if there exists $\mathcal{A}^{-1} \in \mathbb{R}^{m \times m \times C}$ such that $\mathcal{A} \star_c \mathcal{A}^{-1} = \mathcal{I}_{m,C}$.

DEFINITION 3.4 (f-symmetry and f-positive-definiteness). A square tensor $\mathcal{A} \in \mathbb{R}^{m \times m \times C}$ is called f-symmetric if all frontal slices $\widehat{\mathcal{A}}^{(k)}$ are symmetric matrices. It is f-positive-definite (resp. f-positive-semidefinite) if each $\widehat{\mathcal{A}}^{(k)}$ is symmetric positive definite (resp. symmetric positive-semidefinite).

These concepts enable a consistent generalization of classical matrix operations to third-order tensors while preserving properties such as orthogonality, symmetry, and positive definiteness in the DCT domain. They form the algebraic foundation for the TCP-ViT architecture developed in Section 5.

4 Standard Vision Transformer Before introducing the tensorized architecture, we recall the standard Vision Transformer [3] and establish the notation that will serve as the basis for the c-product generalization. All operations in this section are matrix-based and operate on vectorized patch representations.

4.1 Patch Embedding Let $\mathcal{I} \in \mathbb{R}^{H_{\text{img}} \times W_{\text{img}} \times C}$ denote an input image with C channels. The image is partitioned into $N = H_{\text{img}} W_{\text{img}} / P^2$ non-overlapping patches of size $P \times P$. Each patch is flattened into a vector of dimension $d_{\text{eff}} = P^2 C$ and projected to an embedding space via a learnable matrix $W_E \in \mathbb{R}^{d_{\text{eff}} \times d_{\text{eff}}}$:

$$X_0 = [\mathbf{x}_{\text{cls}}; \mathbf{x}_1; \dots; \mathbf{x}_N] + E_{\text{pos}} \in \mathbb{R}^{(N+1) \times d_{\text{eff}}}, \quad (4.1)$$

where $\mathbf{x}_{\text{cls}} \in \mathbb{R}^{d_{\text{eff}}}$ is a learnable classification token and $E_{\text{pos}} \in \mathbb{R}^{(N+1) \times d_{\text{eff}}}$ is a learnable positional embedding.

4.2 Scaled Dot-Product Attention Given an input $X \in \mathbb{R}^{(N+1) \times d_{\text{eff}}}$, the query, key, and value matrices are obtained via linear projections:

$$Q = XW_Q, \quad K = XW_K, \quad V = XW_V, \quad (4.2)$$

where $W_Q, W_K, W_V \in \mathbb{R}^{d_{\text{eff}} \times d_h}$ are learnable weight matrices and $d_h = d_{\text{eff}}/H$ is the per-head dimension. The scaled dot-product attention is defined as

$$\text{Attention}(Q, K, V) = \text{softmax}\left(\frac{QK^\top}{\sqrt{d_h}}\right)V \in \mathbb{R}^{(N+1) \times d_h}. \quad (4.3)$$

The softmax is applied row-wise, so that each row of the attention matrix sums to one.

4.3 Multi-Head Self-Attention With H attention heads, the multi-head self-attention (MHSA) is

$$\text{MHSA}(X) = [O_1; \dots; O_H]W_O \in \mathbb{R}^{(N+1) \times d_{\text{eff}}}, \quad (4.4)$$

where each head output $O_h = \text{Attention}(XW_{Q,h}, XW_{K,h}, XW_{V,h}) \in \mathbb{R}^{(N+1) \times d_h}$, the concatenation $[\cdot]$ is along the column dimension, and $W_O \in \mathbb{R}^{d_{\text{eff}} \times d_{\text{eff}}}$ is a learnable output projection.

4.4 Feed-Forward Network and Layer Normalization Each Transformer layer applies a two-layer feed-forward network (FFN) with expansion ratio r_{ff} and GELU activation:

$$\text{FFN}(X) = \phi(XW_1)W_2, \quad (4.5)$$

where $W_1 \in \mathbb{R}^{d_{\text{eff}} \times d_{\text{ff}}}$, $W_2 \in \mathbb{R}^{d_{\text{ff}} \times d_{\text{eff}}}$, $d_{\text{ff}} = r_{\text{ff}} \cdot d_{\text{eff}}$, and ϕ denotes the element-wise GELU activation.

Layer normalization (LN) is applied with learnable scale and shift vectors $\gamma, \beta \in \mathbb{R}^{d_{\text{eff}}}$.

A full Transformer block maps $X_{\ell-1}$ to X_ℓ via:

$$Y_\ell = X_{\ell-1} + \text{MHSA}(\text{LN}(X_{\ell-1})), \quad (4.6)$$

$$X_\ell = Y_\ell + \text{FFN}(\text{LN}(Y_\ell)). \quad (4.7)$$

4.5 Parameter Count For a single Transformer layer operating at dimension $\delta = d_{\text{eff}}$, the parameter count (excluding biases) is:

$$\Theta_{\text{layer}}^{\text{Std}}(\delta) = \underbrace{4\delta^2}_{\text{MHSA: } W_Q, W_K, W_V, W_O} + \underbrace{2r_{\text{ff}}\delta^2}_{\text{FFN: } W_1, W_2} + \underbrace{4\delta}_{\text{LN: } \gamma, \beta \times 2} = (4 + 2r_{\text{ff}})\delta^2 + 4\delta. \quad (4.8)$$

This $O(\delta^2)$ scaling is the fundamental cost that the c-product framework reduces by a factor of C , as shown in Section 6.

5 The TCP-ViT Architecture We now lift each component of the standard ViT to the tensor setting by replacing matrix multiplication with the tensor cosine product \star_c . The key idea is to represent each patch as a third-order tensor $\mathcal{X}_i \in \mathbb{R}^{d \times C}$ (with $d = P^2$) rather than a flattened vector $\mathbf{x}_i \in \mathbb{R}^{d_{\text{eff}}}$ (with $d_{\text{eff}} = P^2C$). All operations are then performed via the c-product, which couples the C channels through the fixed orthogonal DCT at zero parametric cost.

5.1 Tensor Operations for Vision Transformers DEFINITION 5.1 (t-Linear). *Given an input tensor $\mathcal{X} \in \mathbb{R}^{N \times d \times C}$ and a weight tensor $\mathcal{W} \in \mathbb{R}^{d \times d' \times C}$, the tensor linear projection is*

$$\text{t-Linear}(\mathcal{X}; \mathcal{W}) = \mathcal{X} \star_c \mathcal{W} \in \mathbb{R}^{N \times d' \times C}. \quad (5.1)$$

This operation generalizes the matrix multiplication XW to the tensor setting. In the DCT domain, it decomposes into C independent matrix multiplications: $\widehat{\mathcal{X}}^{(k)} \widehat{\mathcal{W}}^{(k)}$ for $k = 1, \dots, C$. The cross-channel coupling is handled implicitly by the DCT/IDCT pair at zero parametric cost.

DEFINITION 5.2 (t-Softmax). *Given a tensor $\mathcal{S} \in \mathbb{R}^{N \times N \times C}$, the tensor softmax is defined slice-wise in the transform domain:*

$$\text{t-Softmax}(\mathcal{S})_{ijk} = \frac{\exp(\widehat{\mathcal{S}}_{ijk})}{\sum_{\ell=1}^N \exp(\widehat{\mathcal{S}}_{i\ell k})}, \quad \forall i, k, \quad (5.2)$$

where $\widehat{\mathcal{F}}^{(k)}$ denotes the k -th frontal slice in the DCT domain.

The normalization is performed independently for each token i and each frontal slice k in the transform domain. Since the C slices are decoupled in the DCT domain, the attention weights of each frequency component are computed independently, yielding a block-diagonal structure in the attention operator.

DEFINITION 5.3 (t-Attention). Given query, key, and value tensors $\mathcal{Q}, \mathcal{K}, \mathcal{V} \in \mathbb{R}^{N \times d_h \times C}$, the tensor scaled attention is

$$\text{t-Attention}(\mathcal{Q}, \mathcal{K}, \mathcal{V}) = \text{t-Softmax}\left(\frac{1}{\sqrt{d_h}} \mathcal{Q} \star_c \mathcal{K}^{\top c}\right) \star_c \mathcal{V} \in \mathbb{R}^{N \times d_h \times C}, \quad (5.3)$$

where $\mathcal{K}^{\top c} \in \mathbb{R}^{d_h \times N \times C}$ is the c -transpose (Definition 3.2).

DEFINITION 5.4 (t-MHSA). Given an input $\mathcal{X} \in \mathbb{R}^{N \times d \times C}$, H attention heads with $d_h = d/H$, and learnable weight tensors

$$\mathcal{W}_{Q,h}, \mathcal{W}_{K,h}, \mathcal{W}_{V,h} \in \mathbb{R}^{d \times d_h \times C}, \quad h = 1, \dots, H,$$

the tensor multi-head self-attention is

$$\text{t-MHSA}(\mathcal{X}) = [\mathcal{O}_1; \dots; \mathcal{O}_H]_{(2)} \star_c \mathcal{W}_O \in \mathbb{R}^{N \times d \times C}, \quad (5.4)$$

where $\mathcal{W}_O \in \mathbb{R}^{d \times d \times C}$, $[\cdot]_{(2)}$ denotes concatenation along mode 2, and each head output is

$$\mathcal{O}_h = \text{t-Attention}(\mathcal{X} \star_c \mathcal{W}_{Q,h}, \mathcal{X} \star_c \mathcal{W}_{K,h}, \mathcal{X} \star_c \mathcal{W}_{V,h}) \in \mathbb{R}^{N \times d_h \times C}.$$

Correspondence with the standard ViT. In the standard ViT (Section 4.3), each projection $W_{Q,h} \in \mathbb{R}^{d_{\text{eff}} \times d_h}$ operates on the full flattened vector of dimension $d_{\text{eff}} = dC$, requiring $d_{\text{eff}} \cdot d_h = dC \cdot d_h$ parameters per head per projection. In the c -product formulation, the weight tensor $\mathcal{W}_{Q,h} \in \mathbb{R}^{d \times d_h \times C}$ contains only $d \cdot d_h \cdot C$ entries, but crucially these entries operate on the *reduced* dimension d per slice rather than the full dimension dC . This yields a $1/C$ parameter reduction per projection, as formalized in Section 6.

DEFINITION 5.5 (t-LayerNorm). Given $\mathcal{X} \in \mathbb{R}^{N \times d \times C}$ and learnable tensors $\boldsymbol{\gamma}, \boldsymbol{\beta} \in \mathbb{R}^{1 \times d \times C}$, the tensor layer normalization is applied slice-wise in the transform domain:

$$\text{t-LN}(\widehat{\mathcal{X}})_{ijk} = \gamma_{jk} \cdot \frac{\widehat{\mathcal{X}}_{ijk} - \widehat{\mu}_{ik}}{\widehat{\sigma}_{ik} + \varepsilon} + \beta_{1jk}, \quad (5.5)$$

where, for each token i and frontal slice k in the DCT domain:

$$\widehat{\mu}_{ik} = \frac{1}{d} \sum_{j=1}^d \widehat{\mathcal{X}}_{ijk}, \quad \widehat{\sigma}_{ik} = \sqrt{\frac{1}{d} \sum_{j=1}^d (\widehat{\mathcal{X}}_{ijk} - \widehat{\mu}_{ik})^2}.$$

Normalization is computed for each token–slice pair (i, k) independently in the transform domain, preserving the full tensor structure. Since the DCT is an orthogonal transform, $\|\Phi_C \mathbf{x}\|_2 = \|\mathbf{x}\|_2$, the norms of the activations are preserved across domains, ensuring comparable conditioning in each slice.

DEFINITION 5.6 (t-FFN). Given $\mathcal{X} \in \mathbb{R}^{N \times d \times C}$ and weight tensors $\mathcal{W}_1 \in \mathbb{R}^{d \times d_{\text{ff}} \times C}$, $\mathcal{W}_2 \in \mathbb{R}^{d_{\text{ff}} \times d \times C}$ with $d_{\text{ff}} = r_{\text{ff}} \cdot d$, the tensor feed-forward network is

$$\text{t-FFN}(\mathcal{X}) = \phi(\mathcal{X} \star_c \mathcal{W}_1) \star_c \mathcal{W}_2 \in \mathbb{R}^{N \times d \times C}, \quad (5.6)$$

where ϕ denotes the element-wise GELU activation.

5.2 Patch Tensorization Let $\mathcal{I} \in \mathbb{R}^{H_{\text{img}} \times W_{\text{img}} \times C}$ be an input image. We partition it into $N = H_{\text{img}} W_{\text{img}} / P^2$ non-overlapping patches and represent each patch as a matrix $X_i \in \mathbb{R}^{P^2 \times C}$, where $P^2 = d$ is the number of spatial positions within the patch and C is the number of channels. The full set of patches is stacked as a third-order tensor:

$$\mathcal{X} \in \mathbb{R}^{N \times d \times C}, \quad d = P^2. \quad (5.7)$$

Mode 1 indexes the N patches, mode 2 the d spatial positions within each patch, and mode 3 the C channels.

Comparison with the standard ViT. The standard ViT flattens each patch to a vector $\mathbf{x}_i \in \mathbb{R}^{d_{\text{eff}}}$ with $d_{\text{eff}} = dC = P^2 C$, yielding a matrix $X \in \mathbb{R}^{N \times d_{\text{eff}}}$. The TCP-ViT preserves the two-dimensional structure $d \times C$ within each patch, enabling the c -product to exploit cross-channel correlations algebraically.

5.3 Tensor Embedding A learnable classification tensor $\mathcal{T}_{\text{cls}} \in \mathbb{R}^{1 \times d \times C}$ is prepended along mode 1, and a positional tensor $\mathcal{E} \in \mathbb{R}^{(N+1) \times d \times C}$ is added:

$$\mathcal{X}_0 = [\mathcal{T}_{\text{cls}}; \mathcal{X}]_{(1)} + \mathcal{E} \in \mathbb{R}^{(N+1) \times d \times C}. \quad (5.8)$$

5.4 TCP-ViT Transformer Block Each of the L TCP-ViT blocks maps $\mathcal{X}_{\ell-1} \in \mathbb{R}^{(N+1) \times d \times C}$ to $\mathcal{X}_\ell \in \mathbb{R}^{(N+1) \times d \times C}$ via:

$$\mathcal{Y}_\ell = \mathcal{X}_{\ell-1} + \text{t-MHSA}(\text{t-LN}(\mathcal{X}_{\ell-1})), \quad (5.9)$$

$$\mathcal{X}_\ell = \mathcal{Y}_\ell + \text{t-FFN}(\text{t-LN}(\mathcal{Y}_\ell)). \quad (5.10)$$

Every operation maps $\mathbb{R}^{(N+1) \times d \times C}$ to $\mathbb{R}^{(N+1) \times d \times C}$, ensuring that the tensor structure is preserved through all L layers without any flattening or reshaping.

Algorithm 1 TCP-ViT Forward Pass

Require: Image $\mathcal{I} \in \mathbb{R}^{H_{\text{img}} \times W_{\text{img}} \times C}$, L blocks, weight tensors $\{\mathcal{W}_{Q,h}^\ell, \mathcal{W}_{K,h}^\ell, \mathcal{W}_{V,h}^\ell, \mathcal{W}_O^\ell, \mathcal{W}_1^\ell, \mathcal{W}_2^\ell\}_{\ell,h}$

- 1: $\mathcal{X} \leftarrow \text{Patchify}(\mathcal{I}) \in \mathbb{R}^{N \times d \times C}$ $\triangleright d = P^2, N = H_{\text{img}}W_{\text{img}}/P^2$
- 2: $\mathcal{X}_0 \leftarrow [\mathcal{T}_{\text{cls}}; \mathcal{X}]_{(1)} + \mathcal{E}$ $\triangleright \in \mathbb{R}^{(N+1) \times d \times C}$
- 3: **for** $\ell = 1$ to L **do**
- 4: $\tilde{\mathcal{X}} \leftarrow \text{t-LN}(\mathcal{X}_{\ell-1})$ \triangleright Normalize once, reuse for all heads
- 5: **for** $h = 1$ to H **do**
- 6: $\mathcal{Q}_h \leftarrow \tilde{\mathcal{X}} \star_c \mathcal{W}_{Q,h}^\ell$ $\triangleright \in \mathbb{R}^{(N+1) \times d_h \times C}$
- 7: $\mathcal{K}_h \leftarrow \tilde{\mathcal{X}} \star_c \mathcal{W}_{K,h}^\ell$
- 8: $\mathcal{V}_h \leftarrow \tilde{\mathcal{X}} \star_c \mathcal{W}_{V,h}^\ell$
- 9: $\mathcal{S}_h \leftarrow \frac{1}{\sqrt{d_h}} \mathcal{Q}_h \star_c \mathcal{K}_h^\top$ $\triangleright \in \mathbb{R}^{(N+1) \times (N+1) \times C}$
- 10: $\mathcal{O}_h \leftarrow \text{t-Softmax}(\mathcal{S}_h) \star_c \mathcal{V}_h$ $\triangleright \in \mathbb{R}^{(N+1) \times d_h \times C}$
- 11: **end for**
- 12: $\mathcal{Y}_\ell \leftarrow \mathcal{X}_{\ell-1} + [\mathcal{O}_1; \dots; \mathcal{O}_H]_{(2)} \star_c \mathcal{W}_O^\ell$ \triangleright Residual + output projection
- 13: $\mathcal{H} \leftarrow \phi(\text{t-LN}(\mathcal{Y}_\ell) \star_c \mathcal{W}_1^\ell)$ $\triangleright \in \mathbb{R}^{(N+1) \times d_H \times C}$
- 14: $\mathcal{X}_\ell \leftarrow \mathcal{Y}_\ell + \mathcal{H} \star_c \mathcal{W}_2^\ell$ $\triangleright \in \mathbb{R}^{(N+1) \times d \times C}$
- 15: **end for**
- 16: **return** \mathcal{X}_L

5.5 Algorithmic Description REMARK 1 (Lossless factorization). *Unlike pruning, quantization, or low-rank approximation methods, the c-product factorization introduces no approximation error. Since $\Phi_C^\top \Phi_C = I_C$, the mapping $\mathcal{X} \mapsto \text{IDCT}_3(\widehat{\mathcal{W}}^{(k)} \cdot \widehat{\mathcal{X}}^{(k)})$ is exact for any choice of learned weights $\widehat{\mathcal{W}}^{(k)}$. The parameter reduction arises from structural constraints on the weight tensor (block-diagonal structure in the DCT domain), not from information discarding.*

6 Theoretical Analysis

6.1 Parameter Efficiency We compare the parameter counts of the TCP-ViT and the standard ViT. The TCP-ViT operates on tensors $\mathcal{X} \in \mathbb{R}^{N \times d \times C}$, while the standard ViT operates on the flattened representation $X \in \mathbb{R}^{N \times dC}$. Both architectures process the same amount of information per token.

6.1.1 Multi-Head Self-Attention. With H heads and per-head dimension $d_h = d/H$, Table 6.1 compares the weight dimensions.

TCP-ViT count: The H heads contribute $3H \cdot d \cdot d_h C = 3d^2C$ parameters (since $Hd_h = d$), plus d^2C for \mathcal{W}_O :

$$\Theta_{\text{MHSA}}^{\text{c-ViT}} = 4d^2C. \quad (6.1)$$

Standard count: $3H \cdot (dC)(d_h C) = 3d^2C^2$, plus $(dC)^2 = d^2C^2$ for W_O :

$$\Theta_{\text{MHSA}}^{\text{Std}} = 4d^2C^2. \quad (6.2)$$

Ratio: $\Theta_{\text{MHSA}}^{\text{c-ViT}} / \Theta_{\text{MHSA}}^{\text{Std}} = 1/C$.

TABLE 6.1
MHSA weight dimensions. Each projection is listed per head; the total count sums over all H heads.

Projection	TCP-ViT weight tensor	Std-ViT weight matrix
$\mathcal{W}_{Q,h}$	$\mathbb{R}^{d \times d_h \times C}$	$\mathbb{R}^{dC \times d_h C}$
$\mathcal{W}_{K,h}$	$\mathbb{R}^{d \times d_h \times C}$	$\mathbb{R}^{dC \times d_h C}$
$\mathcal{W}_{V,h}$	$\mathbb{R}^{d \times d_h \times C}$	$\mathbb{R}^{dC \times d_h C}$
\mathcal{W}_O	$\mathbb{R}^{d \times d \times C}$	$\mathbb{R}^{dC \times dC}$

6.1.2 Feed-Forward Network. With expansion ratio r_{ff} and hidden dimension $d_{\text{ff}} = r_{\text{ff}} \cdot d$, Table 6.2 compares the weight dimensions.

TABLE 6.2
FFN weight dimensions for TCP-ViT and standard ViT.

Projection	TCP-ViT weight tensor	Std-ViT weight matrix
\mathcal{W}_1	$\mathbb{R}^{d \times d_{\text{ff}} \times C}$	$\mathbb{R}^{dC \times d_{\text{ff}} C}$
\mathcal{W}_2	$\mathbb{R}^{d_{\text{ff}} \times d \times C}$	$\mathbb{R}^{d_{\text{ff}} C \times dC}$

TCP-ViT count:

$$\Theta_{\text{FFN}}^{\text{c-ViT}} = 2 r_{\text{ff}} d^2 C. \quad (6.3)$$

Standard count:

$$\Theta_{\text{FFN}}^{\text{Std}} = 2 r_{\text{ff}} d^2 C^2. \quad (6.4)$$

Ratio: $\Theta_{\text{FFN}}^{\text{c-ViT}} / \Theta_{\text{FFN}}^{\text{Std}} = 1/C$.

6.1.3 Layer Normalization. Each t-LayerNorm has learnable tensors $\gamma, \beta \in \mathbb{R}^{1 \times d \times C}$. A TCP-ViT block uses two normalizations:

$$\Theta_{\text{LN}}^{\text{c-ViT}} = 2 \times 2 \cdot dC = 4dC. \quad (6.5)$$

The standard ViT has $\gamma, \beta \in \mathbb{R}^{dC}$ per normalization:

$$\Theta_{\text{LN}}^{\text{Std}} = 2 \times 2 \cdot dC = 4dC. \quad (6.6)$$

Ratio: 1 (normalization parameters scale linearly, so no quadratic gain).

Total per layer.

$$\Theta_{\text{layer}}^{\text{c-ViT}} = (4 + 2r_{\text{ff}}) d^2 C + 4dC, \quad (6.7)$$

$$\Theta_{\text{layer}}^{\text{Std}} = (4 + 2r_{\text{ff}}) d^2 C^2 + 4dC. \quad (6.8)$$

Over L layers, the dominant quadratic terms yield:

$$\frac{\Theta_{\text{layer}}^{\text{c-ViT}}}{\Theta_{\text{layer}}^{\text{Std}}} \xrightarrow{d \gg 1} \frac{1}{C}. \quad (6.9)$$

This result is independent of the depth L , the number of heads H , and the FFN expansion ratio r_{ff} : the c-product framework yields a uniform $1/C$ parameter reduction across all linear components.

The $1/C$ reduction originates from a fundamental algebraic property of the c-product. In the standard ViT, every learnable linear map operates on the full flattened vector of dimension dC , so that each weight

TABLE 6.3

Per-layer parameter comparison between TCP-ViT and standard ViT. Input tensor $\mathcal{X} \in \mathbb{R}^{N \times d \times C}$, standard input $X \in \mathbb{R}^{N \times d}$. Expansion ratio r_{ff} , H heads, $d_h = d/H$, $d_{\text{ff}} = r_{\text{ff}}d$.

Component	TCP-ViT tensor size	TCP-ViT params	Std params	Ratio
$\mathcal{W}_{Q,h} (\times H)$	$\mathbb{R}^{d \times d_h \times C}$	$d^2 C$	$d^2 C^2$	$1/C$
$\mathcal{W}_{K,h} (\times H)$	$\mathbb{R}^{d \times d_h \times C}$	$d^2 C$	$d^2 C^2$	$1/C$
$\mathcal{W}_{V,h} (\times H)$	$\mathbb{R}^{d \times d_h \times C}$	$d^2 C$	$d^2 C^2$	$1/C$
\mathcal{W}_O	$\mathbb{R}^{d \times d \times C}$	$d^2 C$	$d^2 C^2$	$1/C$
MHSA total	—	$4 d^2 C$	$4 d^2 C^2$	$1/C$
\mathcal{W}_1	$\mathbb{R}^{d \times d_{\text{ff}} \times C}$	$r_{\text{ff}} d^2 C$	$r_{\text{ff}} d^2 C^2$	$1/C$
\mathcal{W}_2	$\mathbb{R}^{d_{\text{ff}} \times d \times C}$	$r_{\text{ff}} d^2 C$	$r_{\text{ff}} d^2 C^2$	$1/C$
FFN total	—	$2 r_{\text{ff}} d^2 C$	$2 r_{\text{ff}} d^2 C^2$	$1/C$
$\boldsymbol{\gamma}, \boldsymbol{\beta} (\times 2)$	$\mathbb{R}^{1 \times d \times C}$ each	$4 d C$	$4 d C$	1
Total per layer	—	$(4+2r_{\text{ff}}) d^2 C$	$(4+2r_{\text{ff}}) d^2 C^2$	$1/C$

matrix has $O(d^2 C^2)$ entries. The c-product framework replaces each such matrix by a third-order weight tensor $\mathcal{W} \in \mathbb{R}^{d \times d \times C}$ with $O(d^2 C)$ entries. The cross-channel coupling that, in the standard setting, requires $O(C)$ additional parameters per connection is handled *implicitly* by the fixed orthogonal DCT matrix Φ_C and its inverse Φ_C^\top , which introduce zero learnable parameters. Since $\Phi_C^\top \Phi_C = I_C$, this factorization is exact: no information is lost, and no approximation is introduced.

6.2 Computational Complexity The FLOPs for a single TCP-ViT layer consist of C independent matrix multiplications at dimension d , plus the DCT/IDCT overhead:

$$F_{\text{layer}}^{\text{TCP-ViT}} = C \cdot F_{\text{layer}}(N, d) + O(N d C \log C), \quad (6.10)$$

where $F_{\text{layer}}(N, d) = (8d^2 + 2r_{\text{ff}}d^2)N + 4N^2d$ is the FLOPs of a standard layer at dimension d . The standard layer operates at dimension dC :

$$F_{\text{layer}}^{\text{Std}} = F_{\text{layer}}(N, dC). \quad (6.11)$$

Let $\alpha = (8 + 2r_{\text{ff}})d$ denote the per-token projection cost coefficient. The exact FLOPs ratio, neglecting the $O(C \log C)$ transform overhead, is:

$$\frac{F^{\text{c-ViT}}}{F^{\text{Std}}} = \frac{\alpha + 4N}{\alpha C + 4N}. \quad (6.12)$$

This ratio approaches $1/C$ in the projection-dominated regime ($\alpha \gg N$, i.e., large embedding dimension d) and approaches 1 in the attention-dominated regime ($N \gg \alpha$, i.e., long sequences).

REMARK 2 (Attention complexity). *The attention computation within each frontal slice remains $O(N^2 d_h)$, i.e., quadratic in the number of tokens N . The c-product framework reduces complexity with respect to the embedding dimension (from dC to d per slice), not the sequence length. This distinction is important: the TCP-ViT does not achieve sub-quadratic attention in N .*

6.3 Training Considerations In TCP-ViT, each learnable weight tensor $\mathcal{W} \in \mathbb{R}^{d \times d' \times C}$ is updated through the c-product structure. Consider a single t-Linear layer (Definition 5.1): $\mathcal{Y} = \mathcal{X} \star_c \mathcal{W}$, where $\mathcal{X} \in \mathbb{R}^{N \times d \times C}$ and $\mathcal{Y} \in \mathbb{R}^{N \times d' \times C}$. By the chain rule applied to the c-product (Definition 3.1), the gradients of the

loss \mathcal{L} with respect to the weight and input tensors are

$$\frac{\partial \mathcal{L}}{\partial \mathcal{W}} = \mathcal{X}^{\top_c} \star_c \frac{\partial \mathcal{L}}{\partial \mathcal{Y}} \in \mathbb{R}^{d \times d' \times C}, \quad (6.13)$$

$$\frac{\partial \mathcal{L}}{\partial \mathcal{X}} = \frac{\partial \mathcal{L}}{\partial \mathcal{Y}} \star_c \mathcal{W}^{\top_c} \in \mathbb{R}^{N \times d \times C}, \quad (6.14)$$

where \mathcal{X}^{\top_c} and \mathcal{W}^{\top_c} denote the c -transposes (Definition 3.2). Since the c -product is built upon the orthogonal DCT matrix Φ_C . Consequently, the Frobenius norms of the gradient tensors (6.13)–(6.14) are identical in the spatial and transform domains. The conditioning of the optimization landscape is therefore preserved across all frontal slices, ensuring that no slice suffers from vanishing or exploding gradients relative to the others.

By the slice-wise property of the c -product (Definition 3.1), the C frontal slices of the weight tensor are updated independently in the transform domain, with cross-channel coupling occurring implicitly through the fixed orthogonal matrices Φ_C and Φ_C^\top at the encoder boundaries. This algebraic structure is analogous to group convolutions, where independent filter groups process channel subsets. The key difference is that the c -product coupling is *exact* and *parameter-free*: the Φ_C/Φ_C^\top pair ensures that inter-channel information is preserved globally despite per-slice independence, without introducing any additional learnable parameters.

7 Numerical Experiments The primary contribution of this work is the algebraic framework developed in Sections 3–6. The experiments in this section serve as a *proof of concept*, with two objectives, verify that the theoretical $1/C$ parameter reduction (Eq. (6.9)) is realized in practice, and assess whether the tensorized model retains competitive accuracy despite the structural constraints imposed by the block-diagonal c -product formulation. We evaluate on classification and segmentation tasks using controlled, small-scale configurations that isolate the effect of the c -product tensorization. Large-scale validation (e.g., ImageNet, deeper architectures) is left to future work.

An important methodological point must be emphasized. The c -product tensorization is not a specific architecture: it is a *general algebraic strategy* that can be applied to any Transformer-based model. Given any standard Transformer operating on flattened tokens $X \in \mathbb{R}^{N \times dC}$, the c -product reformulation replaces every linear projection by the tensor cosine product on the unflattened representation $\mathcal{X} \in \mathbb{R}^{N \times d \times C}$, yielding a $1/C$ parameter reduction with no other architectural change. This strategy applies identically to DeiT, Swin, or any other Transformer variant.

For this reason, comparing TCP-ViT against a *different* architecture (e.g., DeiT or Swin) would conflate two independent factors: the base architecture and the tensorization strategy. The scientifically rigorous comparison is between a given Transformer and its c -product counterpart, with all other design choices held constant. This is exactly the protocol we adopt.

Concretely, we define **Std-ViT** as a vanilla Vision Transformer with the same depth L , number of heads H , expansion ratio r_{ff} , and training protocol as TCP-ViT. The *only* difference is the token representation: Std-ViT flattens each patch to $\mathbf{x}_i \in \mathbb{R}^{d_{\text{eff}}}$ with $d_{\text{eff}} = P^2C$, while TCP-ViT represents each patch as a tensor $\mathcal{X}_i \in \mathbb{R}^{d \times C}$ and processes it via the c -product \star_c . Any observed performance difference therefore isolates the effect of the c -product tensorization.

7.1 Image Classification Datasets. We evaluate on three standard benchmarks:

- **CIFAR-10** [18]: 60,000 colour images (32×32) across 10 categories (50K train / 10K test).
- **SVHN** [22]: over 600,000 digit images (32×32) from Google Street View (10 classes).
- **STL-10** [2]: 13,000 labelled images (96×96 , resized to 32×32) across 10 classes (5K train / 8K test).

To validate architectural properties under controlled conditions, both models are also trained on identically subsampled subsets: 10,000 training and 2,000 test samples per dataset.

Architecture. Both models process $32 \times 32 \times 3$ images with patch size $P = 4$, yielding $N = 64$ patches. Each patch is a tensor $\mathcal{X}_i \in \mathbb{R}^{16 \times 3}$.

- **Std-ViT** flattens each patch to $d_{\text{eff}} = P^2C = 48$ and processes through a single encoder.
- **TCP-ViT** represents each patch as $\mathcal{X}_i \in \mathbb{R}^{d \times C}$ with $d = P^2 = 16$ and $C = 3$, and processes it via the c -product \star_c .

Both use $L = 4$ layers, $H = 4$ heads, and expansion ratio $r_{\text{ff}} = 4$. This yields 119,194 parameters for Std-ViT and 43,114 for TCP-ViT, a ratio of $0.362 \times$ (theoretical: $1/C = 0.333 \times$).

Both models are trained for 150 epochs (subsampled) or 200 epochs (full) using AdamW [20] ($\text{lr} = 0.01$,

weight decay = 0.01) with cosine annealing, batch size 256, gradient clipping at norm 1.0, and mixed-precision training. Data augmentation consists of random cropping (padding 4) and random horizontal flipping. Images are normalized using per-dataset statistics for CIFAR-10 and ImageNet statistics for SVHN and STL-10.

We report top-1 classification accuracy on the test set. Throughout all experimental tables, Δ denotes the absolute performance difference

$$\Delta = \text{metric}(\text{TCP-ViT}) - \text{metric}(\text{Std-ViT}), \quad (7.1)$$

expressed in percentage points. A positive Δ indicates that TCP-ViT outperforms Std-ViT; a negative Δ indicates a performance loss. Best results per row are shown in **bold**.

TABLE 7.1

Classification accuracy on subsampled datasets (10K train / 2K test). TCP-ViT uses $0.362\times$ the parameters of Std-ViT (theoretical: $1/C = 0.333\times$).

Dataset	Std-ViT (%)	TCP-ViT (%)	Δ	Std Params	TCP-ViT Params
CIFAR-10	61.8	63.6	+1.8	119,194	43,114
SVHN	49.8	63.8	+14.0	119,194	43,114
STL-10	52.5	55.9	+3.4	119,194	43,114
Parameter ratio	0.362 \times (theoretical: 0.333 \times)				

Table 7.1 reports the results. Under the subsampled protocol, TCP-ViT matches or exceeds Std-ViT on all three datasets: +1.8% on CIFAR-10, +14.0% on SVHN, and +3.4% on STL-10. These gains are attributed to implicit regularization: Std-ViT, with $2.76\times$ more parameters, exhibits significant overfitting (training loss near zero, diverging validation loss), while TCP-ViT’s reduced capacity constrains the model and yields a more favorable bias–variance trade-off under limited data.

The large gain on SVHN (+14.0%) warrants particular attention. SVHN images contain cluttered backgrounds and variable lighting, which amplify overfitting in the over-parameterized Std-ViT.

TABLE 7.2

Classification accuracy on full CIFAR-10 (50K train / 10K test, 200 epochs). TCP-ViT retains 93.3% of performance with 36.2% of the parameters.

Dataset	Std-ViT (%)	TCP-ViT (%)	Δ	Param ratio
CIFAR-10 (full)	78.7	73.4	−5.3	0.362 \times

Table 7.2 reports the full-scale result. On the complete CIFAR-10, Std-ViT achieves 78.7% while TCP-ViT reaches 73.4% ($\Delta = -5.3\%$). This represents **93.3% performance retention with only 36.2% of the parameters**, a trade-off that is consistent with standard model compression methods, which typically report 3–8% accuracy degradation for 2–3 \times compression. The accuracy gap confirms that when sufficient training data is available, the strict block-diagonal structure in the DCT domain may discard useful cross-frequency interactions that a dense layer can capture.

The c-product decomposes the channel dimension using the DCT, replacing the P^2C -dimensional joint representation with C independent P^2 -dimensional representations. Each frontal slice captures a distinct frequency component: slice $k=1$ corresponds to the channel mean (low-frequency), while subsequent slices encode inter-channel contrasts (higher-frequency). This preserves discriminative features while eliminating the redundancy of the standard flattening $\text{flatten}(P^2, C) \rightarrow \mathbb{R}^{P^2C}$.

7.2 Semantic Segmentation We evaluate on the Oxford-IIIT Pet dataset [24], which contains 7,349 images of 37 cat and dog breeds with pixel-level trimap annotations. Following standard practice, we convert to binary segmentation (foreground vs. background), discarding boundary pixels (label 255). The dataset is split 80/20 into training (5,879) and validation (1,470) sets.

Both models share an identical CNN decoder (4 upsampling stages). The backbone processes 128×128 images with patch size $P = 8$, yielding $N = 256$ patches. Std-ViT uses $d_{\text{eff}} = P^2C = 192$; TCP-ViT operates

on $C = 3$ slices of dimension $d = 64$. Both use $L = 4$ layers, $H = 4$ heads, $r_{\text{ff}} = 2$. After IDCT reconstruction, TCP-ViT outputs features of dimension $dC = 192$, matching the Std-ViT decoder input.

Training protocol. We used: 150 epochs, AdamW ($\text{lr} = 5 \times 10^{-4}$, weight decay 0.01), cosine annealing, cross-entropy loss (ignore index 255), batch size 16, gradient clipping at norm 1.0, mixed-precision. Input resized to 128×128 with ImageNet normalization. Best validation mIoU reported.

Mean IoU (mIoU), mean Dice (mDice), pixel accuracy (PA), and per-class IoU/Dice.

TABLE 7.3

Parameter breakdown for segmentation. The Transformer encoder achieves $0.338\times$, closely matching the theoretical $1/C = 0.333\times$.

Component	Std-ViT	TCP-ViT	Ratio
Total	1,570,978	751,586	$0.478\times$
Backbone	1,275,072	455,680	$0.357\times$
Transformer Encoder(s)	1,188,480	402,048	$0.338\times$
Embeddings & Tokens	86,592	53,632	$0.619\times$
CNN Decoder	295,906	295,906	$1.000\times$

Table 7.3 presents the parameter breakdown. The Transformer encoder achieves a compression ratio of $0.338\times$, closely matching the theoretical $1/C = 1/3 \approx 0.333\times$ from Eq. (6.9). The slight deviation arises from bias terms and LayerNorm parameters, which scale linearly. The CNN decoder is identical ($1.000\times$), confirming it operates on reconstructed features after IDCT. Figure 7.1 provides a visual comparison.

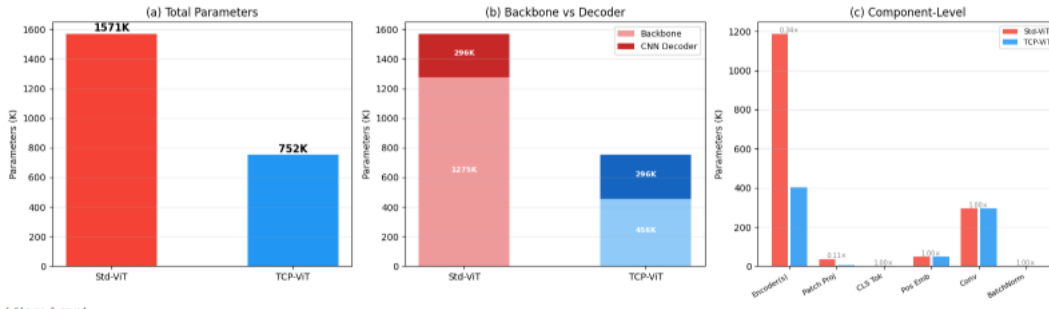


FIG. 7.1. Parameter distribution. (a) Total parameters: TCP-ViT uses $0.478\times$ of Std-ViT. (b) Stacked breakdown. (c) Component-level comparison.

TABLE 7.4

Segmentation performance on Oxford-IIIT Pet. TCP-ViT retains 98.9% of the mIoU with $2.09\times$ fewer parameters. Δ denotes the absolute difference (TCP-ViT – Std-ViT).

Metric	Std-ViT	TCP-ViT	Δ
mIoU (%)	87.8	86.8	-1.0
mDice (%)	93.5	92.9	-0.6
Pixel Acc. (%)	94.2	93.6	-0.6
IoU: Background	84.0	82.7	-1.3
IoU: Foreground (Pet)	91.7	90.9	-0.8
Dice: Background	91.3	90.5	-0.8
Dice: Foreground (Pet)	95.7	95.2	-0.4
Parameters	1,570,978	751,586	$0.478\times$

Table 7.4 summarizes the results. TCP-ViT achieves 86.8% mIoU versus 87.8% for Std-ViT ($\Delta = -1.0\%$) with $2.09\times$ fewer parameters. The degradation is small and consistent across all metrics. The gap is smaller on the foreground class ($\Delta_{\text{IoU}} = -0.8\%$) than on the background ($\Delta_{\text{IoU}} = -1.3\%$), suggesting

that the c-product processing preserves object-level semantics effectively while losing marginal precision on less structured regions.

Figure 7.2 shows the training dynamics over 150 epochs. Both models converge at comparable rates, with TCP-ViT exhibiting slightly higher losses. The mIoU gap stabilizes around 1% after epoch 50. Neither model shows significant overfitting.

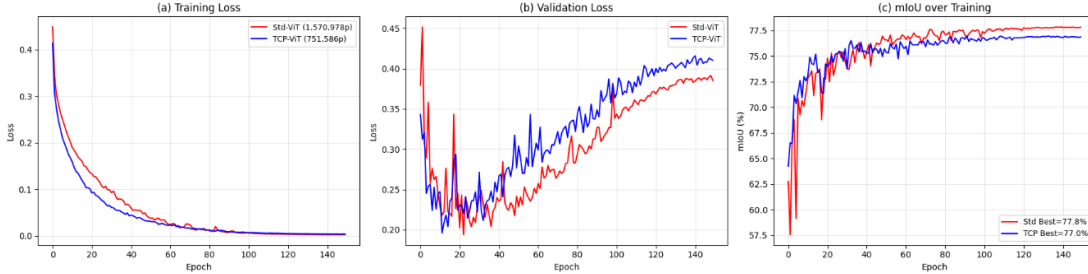


FIG. 7.2. Training dynamics. (a) Training loss, (b) validation loss, (c) mIoU. TCP-ViT (blue) closely tracks Std-ViT (red) with a stable $\sim 1\%$ gap.

Figure 7.3 shows the normalized confusion matrices. Both models achieve high true positive rates ($>90\%$ foreground, $>82\%$ background).

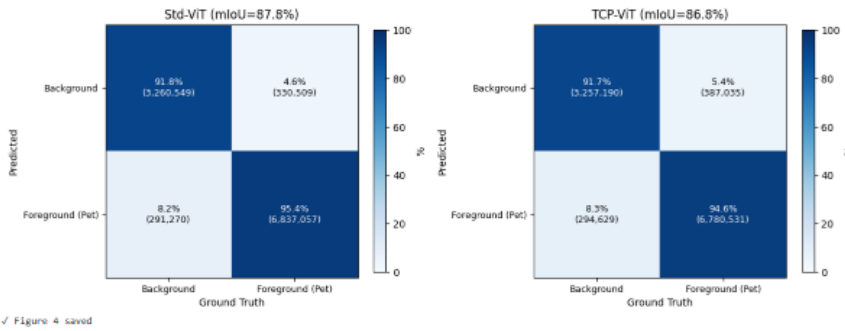


FIG. 7.3. Normalized confusion matrices. Both models show strong diagonal dominance.

Figure 7.4 presents predictions on validation images. Both models produce visually similar masks. TCP-ViT occasionally shows slightly less precise boundaries in regions with complex backgrounds.

Figure 7.5 visualizes error maps. Errors are concentrated along object boundaries for both models, with TCP-ViT showing marginally more boundary errors.

Figure 7.6 presents the parameter-performance trade-off. TCP-ViT reduces parameters by $2.09\times$ while sacrificing only 1.0% mIoU, yielding a compression efficiency of $\eta = \Delta\text{mIoU}/\Delta\text{params} = 1.0\%/52.2\% \approx 0.019$, i.e., less than 0.02% mIoU lost per 1% parameter reduction.

7.3 Discussion We synthesize the experimental findings along four axes: parameter efficiency, data regime sensitivity, task generality, and architectural interpretation.

The theoretical analysis of Section 6.1 predicts a uniform $1/C$ parameter reduction in all linear projections. The experiments confirm this prediction closely: the Transformer encoder compression ratio is $0.362\times$ for classification and $0.338\times$ for segmentation, both near the theoretical $1/C = 1/3 \approx 0.333\times$ (Table 6.3 and Table 7.3). The small deviations are fully accounted for by bias terms and LayerNorm parameters, which scale linearly in dC and thus do not benefit from the $1/C$ reduction. When task-specific components are shared (e.g., the CNN decoder in segmentation), the overall compression ratio is diluted to $0.478\times$, but the Transformer backbone ratio remains near its theoretical value. This confirms that the c-product reduction is exact and architecture-agnostic within the encoder.

The results reveal a clear interaction between model capacity and data availability. Under the subsampled protocol (10K training samples), TCP-ViT *outperforms* Std-ViT on all three datasets ($\Delta = +1.8\%$

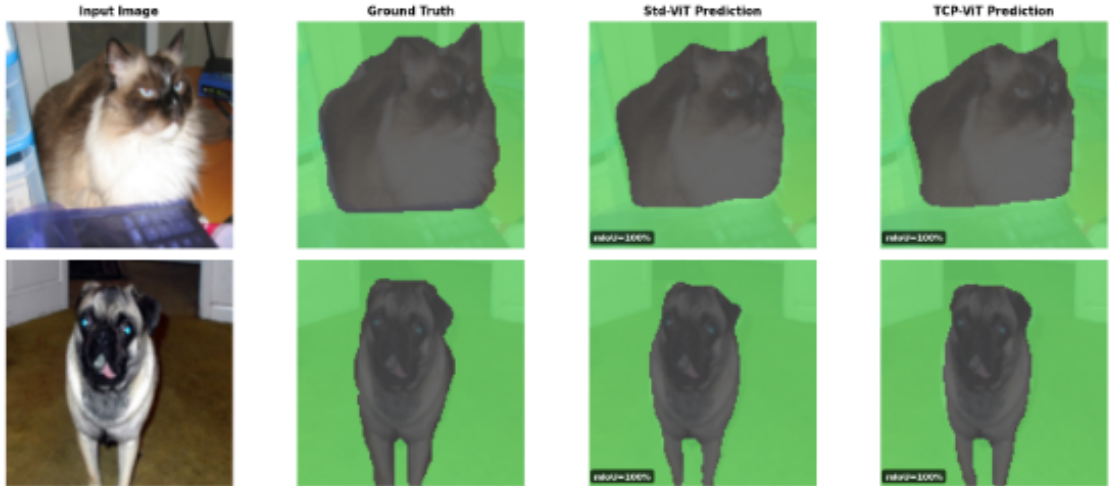


FIG. 7.4. Qualitative results. Columns: input, ground truth, Std-ViT, TCP-ViT. Green overlay: foreground. Per-image mIoU shown on each prediction.

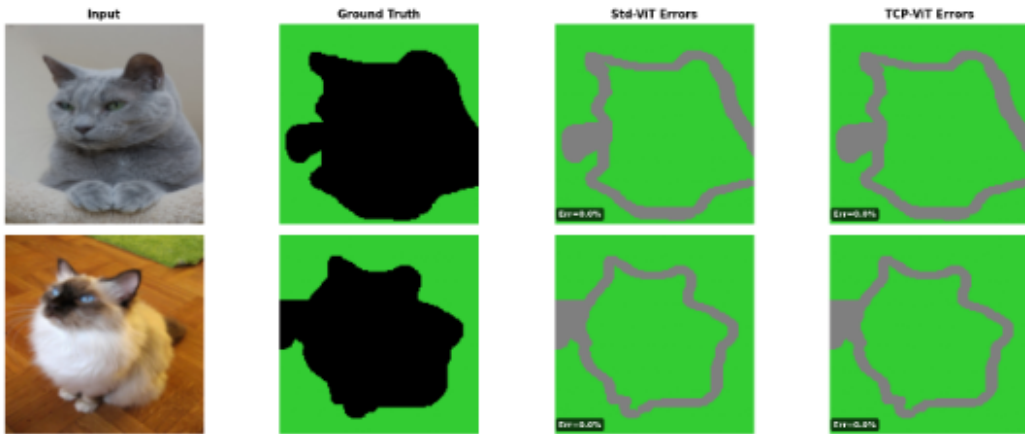


FIG. 7.5. Error maps. Green = correct, red = error, gray = ignored. Errors are concentrated at boundaries for both models.

on CIFAR-10, +14.0% on SVHN, +3.4% on STL-10; Table 7.1). This is consistent with classical bias-variance analysis: the over-parameterized Std-ViT (119K parameters for 10K samples) overfits severely, while TCP-ViT’s reduced capacity acts as an implicit regularizer, constraining the hypothesis space and improving generalization. The effect is most pronounced on SVHN, where cluttered backgrounds and variable lighting amplify overfitting. By contrast, on the full CIFAR-10 (50K samples), Std-ViT achieves 78.7% versus 73.4% for TCP-ViT ($\Delta = -5.3\%$; Table 7.2). With sufficient data, the additional $2.76\times$ parameters of Std-ViT enable it to capture cross-frequency interactions that the block-diagonal c-product structure cannot represent. Nevertheless, TCP-ViT retains 93.3% of the accuracy with only 36.2% of the parameters, a trade-off comparable to standard compression methods that typically report 3–8% degradation for 2–3 \times compression.

Task generality: classification vs. dense prediction. The segmentation experiment demonstrates that the c-product framework extends beyond classification to dense prediction. On the Oxford-IIIT Pet benchmark, TCP-ViT achieves 86.8% mIoU versus 87.8% for Std-ViT ($\Delta = -1.0\%$; Table 7.4), retaining 98.9% of the performance. The accuracy gap is notably smaller than for full-scale classification (-1.0% vs. -5.3%), which can be attributed to two factors: (i) the segmentation task operates at higher resolution (128×128 vs. 32×32), increasing the token count and thus the relative benefit of parameter efficiency; and (ii) the binary segmentation objective may be less sensitive to fine-grained cross-frequency interactions than 10-class classification. The error analysis (Figure 7.5) reveals that degradation is concentrated at object boundaries,

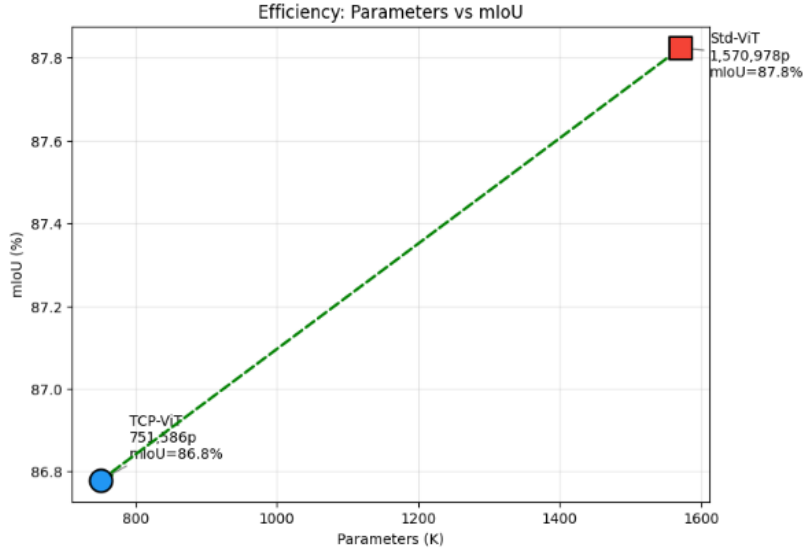


FIG. 7.6. Efficiency trade-off: parameters vs. mIoU. The dashed arrow indicates the compression direction.

consistent with the loss of inter-slice coupling in the DCT domain.

The c-product imposes a *block-diagonal* structure in the DCT domain: each of the C frontal slices is processed by an independent linear map, with cross-channel coupling handled exclusively by the fixed orthogonal matrices Φ_C and Φ_C^\top . This structure has both advantages and limitations. On the positive side, it provides a principled and exact (lossless) parameter reduction, preserved gradient norms due to orthogonality, and a natural decomposition into interpretable frequency components (slice $k=1$ captures the channel mean, higher slices capture inter-channel contrasts). On the negative side, the strict block-diagonal constraint prevents the model from learning arbitrary cross-frequency interactions, which limits expressiveness when sufficient data is available. This trade-off is analogous to group convolutions, where splitting channels into independent groups reduces parameters at the cost of inter-group communication.

Limitations and future directions. Several limitations of the current work should be acknowledged.

1. *Sequential implementation.* The current implementation processes the C frontal slices sequentially. A parallel implementation or multi-stream CUDA kernels is required to realize wall-clock speedups proportional to the theoretical $1/C$ FLOPs ratio.
2. *Task head dilution.* Shared task-specific components (e.g., the CNN decoder in segmentation) are not tensorized and therefore dilute the overall compression from $1/C$ to a higher value. Tensorizing the decoder is a natural extension.
3. *Accuracy gap on large datasets.* The -5.3% gap on full-scale CIFAR-10 suggests that the strict block-diagonal structure discards useful cross-frequency interactions. Future work could explore learnable inter-slice coupling (e.g., a lightweight mixing layer between slices) or partial c-product formulations that relax the block-diagonal constraint while preserving most of the parameter savings.
4. *Scale of experiments.* The current evaluation uses small-scale ViT configurations ($L=4$, $d_{\text{eff}} \leq 192$) on low-resolution benchmarks (32×32 to 128×128). Validation on larger-scale settings (e.g., ImageNet at 224×224 with deeper architectures) is needed to confirm the scalability of the c-product framework.

8 Conclusion We developed a rigorous algebraic framework for tensorizing Vision Transformers based on the tensor cosine product. The central theoretical result is that replacing every linear projection in a standard Transformer by the c-product yields a provable and uniform $1/C$ parameter reduction that is exact (lossless), architecture-agnostic, and independent of the network depth, number of heads, or FFN expansion ratio. The reduction arises from the block-diagonal structure induced by the fixed orthogonal DCT matrix Φ_C , which handles cross-channel coupling at zero parametric cost while preserving gradient norms. Proof-of-concept experiments on classification (CIFAR-10, SVHN, STL-10) and segmentation (Oxford-IIIT Pet) benchmarks confirmed that the theoretical compression ratios are achieved in practice ($0.362\times$ and $0.338\times$ vs. the theoretical $0.333\times$), the tensorized model retains competitive accuracy, and the c-product acts as

an implicit regularizer in low-data regimes. These results validate the algebraic framework and motivate further investigation.

Several directions remain open. On the theoretical side, extensions to learnable inter-slice coupling and partial c-product formulations could relax the block-diagonal constraint while preserving most of the parameter savings. On the practical side, parallel GPU implementations, large-scale validation on ImageNet with deeper architectures, application to other Transformer variants (Swin, DeiT), and extensions to higher-order tensors for video and volumetric data constitute natural next steps. The framework is particularly promising for hyperspectral imaging, where C ranges from tens to hundreds of spectral bands and the $1/C$ reduction becomes correspondingly more significant.

REFERENCES

- [1] Z. Bai, S. M. Cioaca, and L. Reichel, Multilinear systems and tensor Krylov methods, *Numer. Linear Algebra Appl.*, vol. 27, no. 2, e2286, 2020.
- [2] A. Coates, A. Ng, and H. Lee, An analysis of single-layer networks in unsupervised feature learning, in *Proc. AISTATS*, 2011, pp. 215–223.
- [3] A. Dosovitskiy *et al.*, An image is worth 16×16 words: Transformers for image recognition at scale, in *Proc. ICLR*, 2021.
- [4] F. Dufrenois, A. El Ichi, and K. Jbilou, Multilinear discriminant analysis using tensor-tensor products, *J. Math. Model.*, vol. 11, no. 1, pp. 83–101, 2023.
- [5] M. El Guide, A. El Ichi, and K. Jbilou, Discrete cosine transform LSQR and GMRES methods for multidimensional ill-posed problems, *J. Math. Model.*, vol. 10, no. 1, pp. 21–37, 2022.
- [6] A. El Hachimi, K. Jbilou, A. Ratnani, and L. Reichel, A tensor bidiagonalization method for higher-order singular value decomposition with applications, *Numer. Linear Algebra Appl.*, vol. 31, no. 2, e2530, 2024.
- [7] R. Falcao, T. Santos, and M. Carvalho, Efficient Transformers via structured tensor decomposition, *IEEE Trans. Neural Netw. Learn. Syst.*, vol. 33, no. 5, pp. 2034–2047, 2022.
- [8] G. H. Golub and C. F. Van Loan, *Matrix Computations*, 4th ed. Baltimore, MD, USA: Johns Hopkins Univ. Press, 2013.
- [9] Y. Gu, W. Zhou, G. Iacovides, and D. Mandic, TensorLLM: Tensorising multi-head attention for enhanced reasoning and compression in LLMs, arXiv:2501.15674, 2025.
- [10] M. Hached, K. Jbilou, C. Koukouvinos, and M. Mitrouli, A multidimensional principal component analysis via the c-product Golub–Kahan–SVD, *Mathematics*, vol. 9, no. 11, 1249, 2021.
- [11] F. L. Hitchcock, The expression of a tensor or a polyadic as a sum of products, *J. Math. Phys.*, vol. 6, no. 1–4, pp. 164–189, 1927.
- [12] F. E. Keddous, A. Llanza, N. Shvai, and A. Nakib, Vision transformers inference acceleration based on adaptive layer normalization, *Neurocomputing*, vol. 610, p. 128524, 2024. doi: 10.1016/j.neucom.2024.128524.
- [13] S. Khan, M. Naseer, M. Hayat, S. W. Zamir, F. S. Khan, and M. Shah, Transformers in vision: A survey, *ACM Comput. Surv.*, vol. 54, no. 10, pp. 1–41, 2022.
- [14] M. E. Kilmer and C. D. Martin, Factorization strategies for third-order tensors, *Linear Algebra Appl.*, vol. 435, pp. 641–658, 2011.
- [15] M. E. Kilmer, K. Braman, N. Hao, and R. C. Hoover, Third-order tensors as operators on matrices: A theoretical and computational framework with applications in imaging, *SIAM J. Matrix Anal. Appl.*, vol. 34, no. 1, pp. 148–172, 2013.
- [16] Y.-D. Kim, E. Park, S. Yoo, T. Choi, L. Yang, and D. Shin, Compression of deep convolutional neural networks for fast and low power mobile applications, in *Proc. ICLR*, 2016.
- [17] T. G. Kolda and B. W. Bader, Tensor decompositions and applications, *SIAM Rev.*, vol. 51, no. 3, pp. 455–500, 2009.
- [18] A. Krizhevsky, Learning multiple layers of features from tiny images, Tech. Rep., Univ. Toronto, 2009.
- [19] Z. Liu *et al.*, Swin Transformer: Hierarchical vision transformer using shifted windows, in *Proc. ICCV*, 2021, pp. 10012–10022.
- [20] I. Loshchilov and F. Hutter, Decoupled weight decay regularization, in *Proc. ICLR*, 2019.
- [21] L. Martin and B. Smith, Orthogonal transform-based methods for large-scale image processing, *J. Comput. Appl. Math.*, vol. 339, pp. 620–638, 2018.
- [22] Y. Netzer, T. Wang, A. Coates, A. Bissacco, B. Wu, and A. Y. Ng, Reading digits in natural images with unsupervised feature learning, in *NIPS Workshop Deep Learn. Unsupervised Feature Learn.*, 2011.
- [23] A. Novikov, D. Podoprikin, A. Osokin, and D. P. Vetrov, Tensorizing neural networks, in *Proc. NeurIPS*, 2015, pp. 442–450.
- [24] O. M. Parkhi, A. Vedaldi, A. Zisserman, and C. V. Jawahar, Cats and dogs, in *Proc. CVPR*, 2012, pp. 3498–3505.
- [25] P. Sharma, J. T. Ash, and D. Misra, The truth is in there: Improving reasoning in language models with layer-selective rank reduction, in *Proc. ICLR*, 2024.
- [26] K. Su, L. Cao, B. Zhao, N. Li, D. Wu, X. Han, and Y. Liu, DetViT: Discrete cosine transform meet vision transformers, *Neural Netw.*, vol. 172, p. 106139, 2024.
- [27] Z. Tan, W. Wang, and C. Shan, Vision transformers are active learners for image copy detection, *Neurocomputing*, vol. 587, p. 127687, 2024. doi: 10.1016/j.neucom.2024.127687.
- [28] H. Touvron, M. Cord, M. Douze, F. Massa, A. Sablayrolles, and H. Jégou, Training data-efficient image transformers and distillation through attention, in *Proc. ICML*, 2021, pp. 10347–10357.
- [29] H. Wang, Y. Zhu, B. Green, H. Adam, A. Yuille, and L.-C. Chen, Axial-DeepLab: Stand-alone axial-attention for panoptic segmentation, in *Proc. ECCV*, 2020, pp. 108–126.
- [30] J. Guo, K. Han, H. Wu, Y. Tang, X. Chen, Y. Wang, and C. Xu, CMT: Convolutional neural networks meet vision transformers, in *Proc. CVPR*, 2022, pp. 12175–12185.